Fabrication of Core-shell Type Alginate/CNT Composite Adsorbent Beads by Combined Method of Magnetic-field/electrospray: Effect of CNT Orientation on Adsorption of Methylene Blue and Environmental Applications

Razieh Beigmoradi
Department of Chemical Engineering, University of Sistan and Baluchestan, Zahedan, Iran
Yassin Moayedfar
Nanotechnology Research Institute, Faculty of Engineering, University of Sistan and Baluchestan, Zahedan, Iran
Hamed Khosravi
Department of Materials Engineering, University of Sistan and Baluchestan, Zahedan, Iran
Abdolreza Samimi (a.samimi@eng.usb.ac.ir)
Department of Chemical Engineering, University of Sistan and Baluchestan, Zahedan, Iran

Original Research Full Papers

Keywords: Carbon nanotubes (CNT), Calcium-alginate, Methylene blue, Oriented CNT, Adsorption

Posted Date: February 2nd, 2021

DOI: https://doi.org/10.21203/rs.3.rs-175618/v1

Abstract

In the present work, carbon nanotubes (CNT)/alginate composite adsorbent was prepared using combined method of magnetic field/electrospray. The effects of magnetic and electric fields on CNT orientation in the polymeric matrix of adsorbent, and consequently on the methylene blue adsorption were investigated. The adsorbents characteristics and adsorption performance of the six types samples were obtained using field-emission scanning electron microscopy (FE-SEM) and Ultraviolet-visible (UV-Vis) spectroscopy, respectively. The FE-SEM image observations indicated that under the setup's operating condition, the magnetic field could partially orient the CNTs in the polymer matrix while the electrical field had a little effect. The obtained results clearly represented the positive effects of CNT orientation on enhancing the adsorption of methylene blue into the CNT/alginate composite adsorbents. The egg-box model in the CNT/alginate core-shell type beads could explain the adsorption performance of methylene blue solution onto the six types fabricated beads.

Introduction

Industrial development, rapid urbanization, and increasing agricultural products have promoted the need for treating unconventional water sources such as wastewaters. The wastewater treatment, in addition to restoring water to the consumption cycle, also, can prevent environmental pollution. The adsorption processes by particulate solid adsorbents show potential as one of the most powerful ways for the elimination of pollutants in wastewater due to subjecting large adsorption surface area [1–4]. In the recent century, the development of the adsorption technology is owed to nanotechnology and fabrication of the new nanocomposites [5–8].

Carbon nanotubes (CNTs) are considered as ideal adsorption materials due to presenting large specific surface areas, high thermal and chemical stabilities, excellent electronic properties, and exceptional mechanical properties [9–13]. Application of the CNTs in a polymer matrix or a ceramic network represents the effective adsorption efficiency for removing heavy metals and organic pollutants in wastewater [10, 14–18].

Lately, the challenge of using CNTs in nanocomposite materials has been shifted from production, purification, and surface modification methods to sorting, arrangement, and controlling the orientation of the CNTs in the different substrates [19–23]. There are some chemical, electrical, mechanical, and magnetic methods for aligning the CNTs in a polymeric substrate [19, 24–26]. In the mechanical methods, the shear forces on CNT-reinforced nanocomposites would control the CNTs position and their arrangement. Despite simplicity, however, the alignment effectiveness of the mechanical methods is much lower than other techniques [26]. In the chemical methods, the dense arrays of vertically aligned CNTs, so-called CNT forests, are used. The oriented CNT forest is stabilized using capillarity-induced wetting with unmodified complex thermosets or some epoxies [19, 27].

The orientation of the CNTs under electrical field has been reported according to the electrophoresis and dielectrophoresis phenomena. The CNTs, due to the electrical properties such as the quasi-one-dimensional and symmetrical tubular structures, can be aligned in parallel structures using a high electrical field. This method can orient the CNTs in low viscosity polymeric substrates, but, applying the high electric field magnitude limits the possibility of its large-scale employment [9, 28–32].

Calculations and some experimental works found that the CNTs were paramagnetic in the direction of their long axes, and tend to align parallel to the ambient magnetic field [28, 33, 34]. The magnetic susceptibility of the CNTs is highly dependent on the magnetic field direction and temperature. For a successful orientation, the CNTs must prevail on the thermal energy of Brownian motion and the rotation resistance in the viscous polymer solution [35, 36]. Although there are a number of investigations reporting the CNT orientation under the magnetic field, nevertheless, many questions have arisen about the capability of this method in various materials and applications [30, 33, 35–37]. Therefore, more detailed investigations must be carried out regarding the CNTs' alignment in a polymer matrix under the magnetic field and their applications such as in the adsorption of heavy metals or organic pollutants from wastewaters. It seems that in case of synthesizing aligned CNTs dispersed in a polymer matrix, this method might be feasible as an energy efficient and cheap method.

In this study, a novel setup of magnetic field/electrospray was employed to orient the CNTs in the porous calcium alginate-CNTs (CA-CNTs) composite adsorbent beads. To the best knowledge of authors there is no study focusing on combining magnetic and electric fields with aims to align CNTs dispersed in the polymeric adsorbent beads, as well as applying them to eliminate aqueous organic dyes. To investigate the adsorption performance of the prepared absorbents, the sodium alginate-CNTs droplets were electro-sprayed in calcium chloride gelling agent to obtain CA-CNTs core-shell beads, while the magnetic field on sol flow was applied before electrospray. The composite adsorbents were then characterized by Field Emission Scanning Electron Microscope (FESEM), Fourier Transform Infrared spectroscopy (FTIR), and Ultraviolet and Visible spectroscopy (UV-vis). The adsorption studies was done to find out the effects of magnetic and electrical fields on the CNT orientation and, subsequently, methylene blue (MB) removal.

Experimental

Materials

Sodium-alginate (SA) was provided by Sigma-Aldrich Co. (USA). The multi-walled carbon nanotubes (CNT-95% purity) with external diameters between 20 to 45 nm and lengths between 20 to 30 μm were supplied by US Research Nanomaterials Inc. (USA). Figure 1 depicts a FE-SEM image of the CNTs.

Three types of CNTs containing hydroxyl (-OH), carboxyl (-COOH), and amine ($-NH_2$) functional groups were used. FTIR spectra of the CNT powders containing the mentioned functional groups are shown in Fig. 2. As reported in the literature, vibration of hydroxyl groups from intermolecular hydrogen-bonded OH:OH or unbound or free hydroxyl of phenol appears around 3200–3600 cm^{-1}. Furthermore, the

absorbance bands at 1640 – 1630 cm^{-1} are related to the bending or deformation of the hydroxyl groups [38–40]. In Fig. 2b, the absorbance peaks around 1700–1800 cm^{-1}, and the peak at 1556 cm^{-1} resulted from C = O and C-O stretching, respectively. These two absorbance bands and a broadband peak at 3400 cm^{-1} are attributed to the –COOH groups on the external surface of CNTs [37, 38, 41]. For CNT-NH_2 (Fig. 2c), the in-plane bending vibration of N-H appears at 1799 cm^{-1}. The peaks at 1115 cm^{-1} and 3408 cm^{-1} were ascribed to the stretching vibration of C-N and the stretching vibration of N-H, respectively [21, 41, 42].

Methylene blue (MB), as a cationic dye, was selected as adsorbate and provided by Merck Co. (Germany)

Preparation of the SA-CNT suspension

To obtain a most stable SA-CNT suspension, 0.5 wt.% CNT (calculation according to the weight of the SA polymer), containing each of functional group, was initially dispersed in the doubled distilled water. After sonicating for 2 h (34 kHz, Elmasonic P 30 H, Germany), the samples were then centrifuged under 6000 rpm for 45 min (Hettich® EBA 20, Germany) to separate the possible aggregated CNTs. The supernatant liquid was sonicated again for 20 min to obtain partially stable CNT suspension, and 1.5 wt.% SA solution was then added to the latter suspension. The resultant colloidal solution was stirred for 5 h using a magnetic stirrer (Hei-Standard-Germany). At last the sedimentation rate test was conducted on the suspensions for a period time of 16 h to characterize the optimum stable sample.

Magnetic field/electro-spray combined method

Figure 3 shows the picture and a schematic drawing from the lab scale setup of magnetic-field/electro-spray used in this work. The setup includes two hydraulic syringes, a microinfusion pump (WZ-60C2, China), and a calcium chloride solution collector container. Briefly, the SA-CNT solution flow was conducted to a nozzle spinneret (18G) using the microinfusion pump at a flow rate of 50 mL/h. In the tests, a 0–25 kV DC power supply (LD Didactic GmbH, Germany) was used, where its positive charge was connected to the solution's spinneret tip and the collector container was earthed. The distance between spinneret tip and the collector top surface was adjusted to 7.5 cm, and the DC voltage was keep constant at 18 kV to obtain 2.4 V/cm electric field intensity. The SA-CNT was sprayed into the calcium chloride gelling solution and mixed for 10 min to encapsulate the SA-CNT by a solid layer of the CA-CNT. These sample beads were labeled as CA-CNT_{ES}.

To fabricate the gel type calcium alginate beads by the magnetic-mechanical spray (CA-$CNT_{M/MS}$) or magnetic-electrospray (CA-$CNT_{M/ES}$) methods, two magnetic plates of Neodymium (N42 grade with 20mm*40mm*50mm dimensions) were used. In this regard, before the spraying process, the SA-CNT solution was subjected to the uniform magnetic field of strength 318 mT for 2 h.

The beads labeled as CA-CNT_{MS}, were obtained by dripping the SA-CNT solutions under no magnetic and electric fields into gelling agent of calcium chloride. These beads were prepared to compare the effect of

mechanical spraying (MS) with the solely electrospray (ES) or combination of magnetic field (M) and electrospray methods on their adsorption performance.

All the formed CA beads were thoroughly washed with doubled distilled water to make them chloride free. Finally, CA beads were stored under water for further use.

To study the effect of the CNT presence in the adsorbent bead on the methylene blue (MB) adsorption, two control samples of the CA_{MS} and the CA_{ES} were also fabricated without CNT by the mechanical and the electrospray methods, respectively. Some beads were sieved from gelling solution and were frozen in liquid nitrogen for the freeze-drying and then microscopic analysis.

Characterization methods

The surface functional groups of CNTs were determined by a PerkinElmer FTIR spectrophotometer between 400 and 4000 cm^{-1} wavenumbers. The dispersion of CNTs in each bead was evaluated using an optical microscope (OLYMPUS) and a field-emission scanning electron microscopy (FESEM, MIRA3, TESCAN). To prepare the FE-SEM samples and obtain images from the surface or cross-section of the beads, the adsorbents were initially freeze-dried (Dorsatech, Iran) and some of them were then broken. To characterize the adsorption efficiency of MB onto SA-CNT composite, the concentration of MB was characterized in the bulk of solution by the T80/T80 + UV–Vis spectrophotometer (PG Instruments Ltd.).

In the adsorption experiments, the MB solution (50 mg/lit) was prepared and then added to a gel type adsorbent beads at a 3:1 volume ratio. The contact times were set as 0, 5, 30, 60, 120, 240, 480, 960 min and the adsorption of the MB was reported.

One-way analysis of variance (ANOVA) with a Tukey Post hoc test was used for statistical analysis of the MB adsorption onto the fabricated absorbents. For p-value < 0.05 the differences were considered significant.

Results And Discussion

Dispersion and distribution of the CNTs in the polymer solution

Figure 4 shows the results of the sedimentation rate test for the prepared SA-CNT samples. Comparison of the images clearly show that for the suspension containing CNT-NH_2, the stability conditions are disturbed after 4 h, and the CNTs are precipitated as large clusters. This phenomenon occurred for the CNT-OH and CNT-COOH samples after 16 h and 8 h, respectively. These observations imply that the CNT-COOH and CNT-OH samples present relatively more stability than the CNT-NH_2 sample in aqueous suspension. The similar results have been reported in other works, but in different settling rate for CNTs functionalized with carboxyl and hydroxyl groups [40, 43, 44].

Figure 5 shows the CA-CNT adsorbents produced by the stable and unstable suspension of CNT. As can be seen in the figure, the dark spots (white arrows) indicate the presence of CNT clusters demonstrating

the poor dispersion of the CNT in the adsorbent matrix.

The size of beads produced by electrical and mechanical spraying

Figure 6 depicts the beads' size distributions of the CA_{MS} and CA_{ES} adsorbents, which are produced in similar conditions. As shown, the bead diameter spans for the samples produced by electrical and mechanical spraying are 180–580 μm and 1900–2140 μm, respectively. This indicates that the size mode of beads produced by electrospray is smaller as compared to those beads produced by mechanical spray. These results are in agreement with other works representing the effect of electric field on the size reduction of sprayed droplets [45–48].

FE-SEM examinations

As mentioned before, the freeze-drying route was utilized to evaluate the CNTs' distribution in the matrix of each adsorbent. Figure 7 illustrates the bead images before and after the freeze-drying. Besides, the SEM micrographs from the outer surface of the CA-CNT_{MS} and CA-CNT_{ES} beads are also shown in this figure. As can be seen from SEM images, the electrospray and freeze-drying of CA-CNT_{ES} has led to more shrinkage with wrinkled surface, and smaller size of the beads as compared to CA-CNT_{MS}.

Figure 8 shows the SEM images from the outer surfaces of the CA-CNT_{MS}, CA-CNT_{ES}, CA-$CNT_{M/MS}$ and CA-$CNT_{M/ES}$ freeze-dried beads. The preliminary observation of the surfaces morphology indicates that the surface grooves are directional especially for CA-CNT_{ES} (Figs. 8c and 8d) as compared to CA-CNT_{MS} (Fig. 8a). Furthermore, it seems that the traces of CNTs are seen on the surface of CA-CNT_{MS} sample in which the nano-tubes are most probable to be uniformly distributed in the alginate structure (Fig. 8a). For others there is no sign of CNTs on the surface, and therefore, those might be embedded more inside the absorbent beads. In general, it is obvious from the surface morphology of beads that the magnetic and electric fields have affected the structural characteristics of the produced beads.

To investigate the effect of the electrical and the magnetic fields on the arrangement and the orientation of the CNTs in the polymeric matrix, SEM images were taken from the fractured surfaces of the CA-CNT_{ES}, and CA-$CNT_{M/ES}$ samples. As shown in Figs. 9a and 9b it can see that the CNTs have been distributed well in the polymer matrix.

For the CA-CNT_{ES} sample, it looks that the CNTs have no specified orientation, and therefore, the electric field has not been able to orientate the CNTs (Fig. 9a). This would be attributed to insufficient force applied on CNTs for their alignment within the viscous calcium alginate suspension as well as a very short retention time of suspension flow under the electrospray field. For the CA-$CNT_{M/ES}$ sample, however, the CNTs have been partially oriented demonstrating the ability of the magnetic field to orient the CNTs (Fig. 9b) under the specific processing conditions. The similar result for the magnetic field was also reported in the work of Shi *et al.* [49].

MB adsorption onto the beads

As shown in Fig. 10, MB adsorption onto the six fabricated adsorbent beads has been evaluated at different time steps. As seen, the adsorption of the MB is generally increased with the CA-CNTs beads, as compared to the bare CA sample. It is interesting to note that for the samples free from CNTs (i.e. CA_{MS} and CA_{ES}), the MB adsorption is almost same at the early stages, while after about 60 min, it becomes higher for the CA_{MS} sample as compared to CA_{ES} one. In the presence of CNTs the adsorption trends get closer between CA-CNT_{MS} and CA-CNT_{ES}. However, as the effects of magnetic and electric fields, the MB elimination rate trend for CA-$CNT_{M/ES}$ beads is much better, and it achieves the highest adsorption efficiency among five other samples.

SA droplets can acquire the shell and core gel type characteristics when carboxylate groups of the alginate are cross-linked by divalent cations such a calcium. This called the “egg-box” model for the gelation mechanism. The name “egg-box” is used because one divalent cation Ca^{+2} interacts with four –COOH groups [50, 51]. The latter phenomenon, so-called external gelation, may lead to formation of mechanically stable gel network of CA shell around the SA solution core [50–54]. Figure 11 illustrates schematically the egg-box model and the cross sectional views of a produced SA-CA core-shell beads.

The MB species in the bulk of aqueous solution, surrounding the beads, are initially adsorbed onto the CA shell, followed by their molecular diffusions through the porous shell and then being transferred into SA core solution [55]. The same mechanism would also prevail for the CA-CNTs beads. This mechanism has been well detailed in the drug release from calcium alginate beads [54, 56, 57].

As depicted in Fig. 10, the adsorption of MB for all embedded CNT samples initially exhibited a fast uptake. Wang et al, reported that the uptake process of MB for MWCNT is very fast and then showed a steady trend after the equilibration point [58]. It can be concluded that at the early stages of the adsorption the physical interaction of the beads’ surface with MB prevails, and then the migration process would proceed through shell intward the core [55].

To compare more precisely the combined effect of mechanical, magnetically, and electrical spraying, the adsorption trend of the MB species as a function of contact time for the first hour are shown in Figs. 12 and 13, respectively. As seen in Fig. 12, the presence of CNTs and their orientation by magnetic field (M) enhances the adsorption rate in the absence of electric field and under mechanical spray (MS), where the beads are larger. The adsorption efficiency of these three samples have been calculated in 60 min, so that the CA-$CNT_{M/MS}$ sample adsorbs about 30% of the MB. However, this value is about 23% for CA-CNT_{MS} and 19% for CA_{MS}. It is noted that absorbance values of the samples are significant too ($p\text{-value} < 0.05$).

For the samples that electrospray route is employed (Fig. 13), there is a significant difference between the absorption rates of the CA-CNT_{ES} and CA-$CNT_{M/ES}$ samples, as compared to the neat ones ($p\text{-value} < 0.05$). In fact, as an effect of electric field in producing smaller beads, the adsorption mechanism were mainly controlled by the diffusive transport of the MB compounds within the pore network of the nanocomposites and the CNT’s sites [16]. Calculating the adsorption efficiency of the MB onto the CA-CN_{ES} and CA-$CNT_{M/ES}$ beads indicates that in the first hour, about 65% of the MB is adsorbed by the CA-

$CNT_{M/ES}$ bead, and it is approximately 22% and 12% for the CA-CNT_{ES} and neat beads, respectively. It must be noted that in 60 min, the absorbance values of the CA-CNT_{ES} and CA-CNT_{M} samples are not significant (p-value < 0.05).

After 1 hour, the slopes of the adsorption are decreased in all samples. The CA-$CNT_{M/ES}$ bead could remove about 88% of the MB concentration after 16h, and this value is about 67% for the same sample fabricated by the mechanical spraying. In this study, the equilibrium time for the CA-CNTs absorbent is longer than has been reported in other works [58–60]. This could be due to differences in pore tortuosity of the nanocomposites.

These observations confirm that the carbon nanotubes increase the efficiency of the MB adsorption, and their orientation in a polymeric structure can enhance the capability of the adsorption. The similar results have been reported in other experimental works [61, 62].

Conclusions

In the present work, fabrication of CA-CNT composite adsorbents was investigated with an emphasis on the orientation of CNTs in a polymer matrix. In this regard, two mechanical and electrical spraying methods were used. To orient the carbon nanotubes, before the spraying process, the mixture containing the CNT was subjected to the magnetic field. To achieve the high stability and uniformity of the CNT dispersion in the polymer matrix, the CNT with three functional groups (carboxyl, hydroxyl, and amine) was used. The results showed that CNT-COOH was more stable in sodium alginate and uniformly dispersed throughout the matrix when forming adsorbent beads. The morphological studies of the adsorbents showed that although the electric field reduced the size of the adsorbent beads, compared to the adsorbents made by the mechanical spraying, it had no significant effect on the orientation of CNTs. However, the FE-SEM results indicated that the magnetic field could partially align the nanotubes in the polymer matrix. Comparing the adsorption of the MB by the fabricated adsorbents demonstrated that the presence of the CNTs in the adsorbent bead improved the adsorption efficiency. Furthermore, the oriented CNTs increased the MB adsorption, so that the MB adsorption efficiency for the samples made by the electrospray/magnetic field was more than 85%. However, the highest adsorption for the same sample containing random CNT was about 67%. The results revealed that the orientation of the CNTs without increasing their concentration could improve the effectiveness of these nanoparticles, and led to fabricating the cheaper products with higher performance.

Declarations

Ethics approval

Not applicable

Consent to participate

My colleagues and I voluntarily agree to participate in this research study.

Consent for publication

My colleagues and I, all agree that the paper to be published in your journal.

Authors' contributions

Samimi and Beigmoradi contributed to the design the research, and developed the theoretical framework. Moreover, Beigmoradi processed the experimental data and drafted the manuscript. Samimi was involved in planning and supervised the work. He aided in interpreting the results and worked on the final manuscript. Moayedfar manufactured the samples and performed the experiments and all characterization. Khosravi contributed to the implementation of the research, and helped to write the manuscript.

Funding

The authors did not receive support from any organization for the submitted work.

Conflicts of interest/Competing interests

The authors declare that they have no known competing financial interests or personal relationships that could have appeared to influence the work reported in this paper.

Availability of data and material

All data generated or analyzed during this study are included in this published article.

Code availability

Not applicable.

References

1. Matias CA, Vilela PB, Becegato VA, Paulino AT. International Journal of Environmental Research 13 (6):991-1003 (2019)
2. Papegowda PK, Syed AA Isotherm. International Journal of Environmental Research 11 (1):91-98 (2017)
3. Vega-Negron AL, Alamo-Nole L, Perales-Perez O, Gonzalez-Mederos AM, Jusino-Olivencia C, Roman-Velazquez FR. International Journal of Environmental Research 12 (1):59-65 (2018)
4. Fard AK, Rhadfi T, Mckay G, Al-marri M, Abdala A, Hilal N, Hussien MA. Chemical Engineering Journal 293:90-101 (2016)

5. Alizadeh N, Shariati S, Besharati N. International Journal of Environmental Research 11 (2):197-206 (2017)
6. Kong D, Zheng X, Tao Y, Lv W, Gao Y, Zhi L, Yang Q-H. Adsorption 22 (8):1043-1050 (2016)
7. Phasuk A, Srisantitham S, Tuntulani T, Anutrasakda W. Adsorption 24 (2):157-167 (2018)
8. Li Y, Bi H-Y, Jin Y-S. Chemical Engineering Journal 308:78-88 (2017)
9. Beigmoradi R, Aghamiri SF. Journal of Particle Science & Technology 5 (4):123-134 (2019)
10. Fiyadh SS, AlSaadi MA, Jaafar WZ, AlOmar MK, Fayaed SS, Mohd NS, Hin LS, El-Shafie. Journal of Cleaner Production 230:783-793 (2019)
11. Gan D, Dou J, Huang Q, Huang H, Chen J, Liu M, Qi H, Yang Z, Zhang X, Wei Y. Journal of Environmental Chemical Engineering 8 (2):103525 (2020)
12. Herrera-Herrera AV, González-Curbelo MÁ, Hernández-Borges J, Rodríguez-Delgado MÁ. Analytica Chimica Acta 734:1-30 (2012)
13. Li Z, Sellaoui L, Franco D, Netto MS, Georgin J, Dotto GL, Bajahzar A, Belmabrouk H, Bonilla-Petriciolet A, Li Q. Chemical Engineering Journal 389:124467 (2020)
14. Ghaedi M, Khajehsharifi H, Yadkuri AH, Roosta M, Asghari A. Toxicological & Environmental Chemistry 94 (5):873-883 (2012)
15. Mallakpour S, Rashidimoghadam S. Polymer 160:115-125 (2019)
16. Santoso E, Ediati R, Kusumawati Y, Bahruji H, Sulistiono DO, Prasetyoko D. Materials Today Chemistry 16:100233 (2020)
17. Adewunmi, A. A., Ismail, S., & Sultan, A. S. Journal of Inorganic and Organometallic Polymers and Materials, 26(4): 717-737 (2016)
18. Wu, S., Huang, J., Zhuo, C., Zhang, F., Sheng, W., & Zhu, M. Journal of Inorganic and Organometallic Polymers and Materials, 26(3): 632-639 (2016)
19. Beigmoradi R, Samimi A, Mohebbi-Kalhori D. Beilstein journal of nanotechnology 9 (1):415-435 (2018)
20. Cob J, Oliva-Avilés A, Avilés F, Oliva A. Materials Research Express 6 (11):115024 (2019)
21. Su Z, Wang H, Ye X, Tian K, Huang W, He J, Guo Y, Tian X. Composites Part A: Applied Science and Manufacturing 109:402-412 (2018)
22. Adewunmi, A. A., Ismail, S., & Sultan, A. S. Journal of Inorganic and Organometallic Polymers and Materials, 26(4): 717-737 (2016)
23. Hattenhauer, I., Tambosi, P. P., Duarte, C. A., Coelho, L. A. F., Ramos, A., & Pezzin, S. H. Journal of Inorganic and Organometallic Polymers and Materials, 25(4): 627-634 (2015)
24. Razib MABM, Saleh T. Current Nanoscience 15 (4):328-353 (2019)
25. Xie X-L, Mai Y-W, Zhou X-P. Materials science and engineering: R: Reports 49 (4):89-112 (2005)
26. Iakoubovskii K. Central European Journal of Physics 7 (4):645-653 (2009)

27. Li L, Yang Z, Gao H, Zhang H, Ren J, Sun X, Chen T, Kia HG, Peng H. Advanced Materials 23 (32):3730-3735 (2011)
28. Goh PS, Ismail AF, Ng BC. Composites Part A: Applied Science and Manufacturing 56:103-126 (2014)
29. Murugesh AK, Uthayanan A, Lekakou C. Applied Physics A 100 (1):135-144 (2010)
30. Romyen N, Thongyai S, Praserthdam P. Journal of applied polymer science 123 (6):3470-3475 (2012)
31. Singer G, Sinn G, Rennhofer H, Schuller R, Grünewald T, Unterlass M, Windberger U, Lichtenegger H. Composite Structures 215:178-184 (2019)
32. Tran C-D, Le-Cao K, Bui TT. Carbon 155:279-286 (2019)
33. Hu X, Sun J, Peng R, Tang Q, Luo Y, Yu P. Journal of Cleaner Production 242:118423 (2020)
34. Walters DA, Casavant MJ, Qin XC, Huffman CB, Boul PJ, Ericson LM, Haroz EH, O'Connell MJ, Smith K, Colbert DT, Smalley RE. Chemical Physics Letters 338 (1):14-20 (2001)
35. Liu M, Younes H, Hong H, Peterson G. Polymer 166:81-87 (2019)
36. Ciambella J, Stanier DC, Rahatekar SS. Composites Part B: Engineering 109:129-137 (2017)
37. Zarnegar Z, Safari J. International journal of biological macromolecules 75:21-31 (2015)
38. Ţucureanu V, Matei A, Avram AM. Critical reviews in analytical chemistry 46 (6):502-520 (2016)
39. Lin Y-T, Singh R, Kuo S-W, Ko F-H. Materials 9 (6):438 (2016)
40. do Amaral Montanheiro TL, Cristóvan FH, Machado JPB, Tada DB, Durán N, Lemes AP. Journal of Materials Research 30 (1):55-65 (2015)
41. Wulandari S, Widiyandari H, Subagio A. In: Journal of Physics: Conference Series, vol 1. IOP Publishing, p 012005 (2018)
42. Maleki A, Hamesadeghi U, Daraei H, Hayati B, Najafi F, McKay G, Rezaee R. Chemical Engineering Journal 313:826-835 (2017)
43. Ma P-C, Siddiqui NA, Marom G, Kim J-K. Composites Part A: Applied Science and Manufacturing 41 (10):1345-1367 (2010)
44. Zhao Z, Yang Z, Hu Y, Li J, Fan X. Applied Surface Science 276:476-481 (2013)
45. Jaworek A. Powder technology 176 (1):18-35 (2007)
46. Moghadam H, Samimi M, Samimi A, Khorram M. Journal of applied polymer science 118 (3):1288-1296 (2010)
47. Marsh BM, Iyer K, Cooks RG. Journal of The American Society for Mass Spectrometry 30 (10):2022-2030 (2019)
48. Zeeb B, Saberi AH, Weiss J, McClements DJ. Food Hydrocolloids 50:27-36 (2015)
49. Shi D, He P, Zhao P, Guo FF, Wang F, Huth C, Chaud X, Bud'ko SL, Lian J. Composites Part B: Engineering 42 (6):1532-1538 (2011)
50. Braccini I, Pérez S. Biomacromolecules 2 (4):1089-1096 (2001)
51. Sosnik A. ISRN Pharmaceutics 926157 (2014)

52. Omidi J, Khorram M, Samimi A. Journal of applied polymer science 117 (1):322-328 (2010)
53. Gogoi N, Chowdhury D. Journal of Materials Chemistry B 2 (26):4089-4099 (2014)
54. Uyen NTT, Hamid ZAA, Tram NXT, Ahmad N International Journal of Biological Macromolecules 153:1035-1046 (2020)
55. Li Y, Sui K, Liu R, Zhao X, Zhang Y, Liang H, Xia Y. Energy Procedia 16:863-868 (2012)
56. Aslani P, Kennedy RA. Journal of Controlled Release 42 (1):75-82 (1996)
57. Acarturk F, Takka S. Journal of microencapsulation 16 (3):291-302 (1999)
58. Wang B, Gao B, Zimmerman AR, Lee X. Chemical Engineering Research and Design 133:235-242 (2018)
59. Bulut Y, Aydın H. Desalination 194 (1):259-267 (2006)
60. Doğan M, Alkan M, Türkyilmaz A, Özdemir Y. Journal of hazardous materials 109 (1-3):141-148 (2004)
61. Farghali AA, Bahgat M, El Rouby WMA, Khedr MH. Journal of Solution Chemistry 41 (12):2209-2225 (2012)
62. Ai L, Zhang C, Liao F, Wang Y, Li M, Meng L, Jiang J. Journal of Hazardous Materials 198:282-290 (2011)

Figures

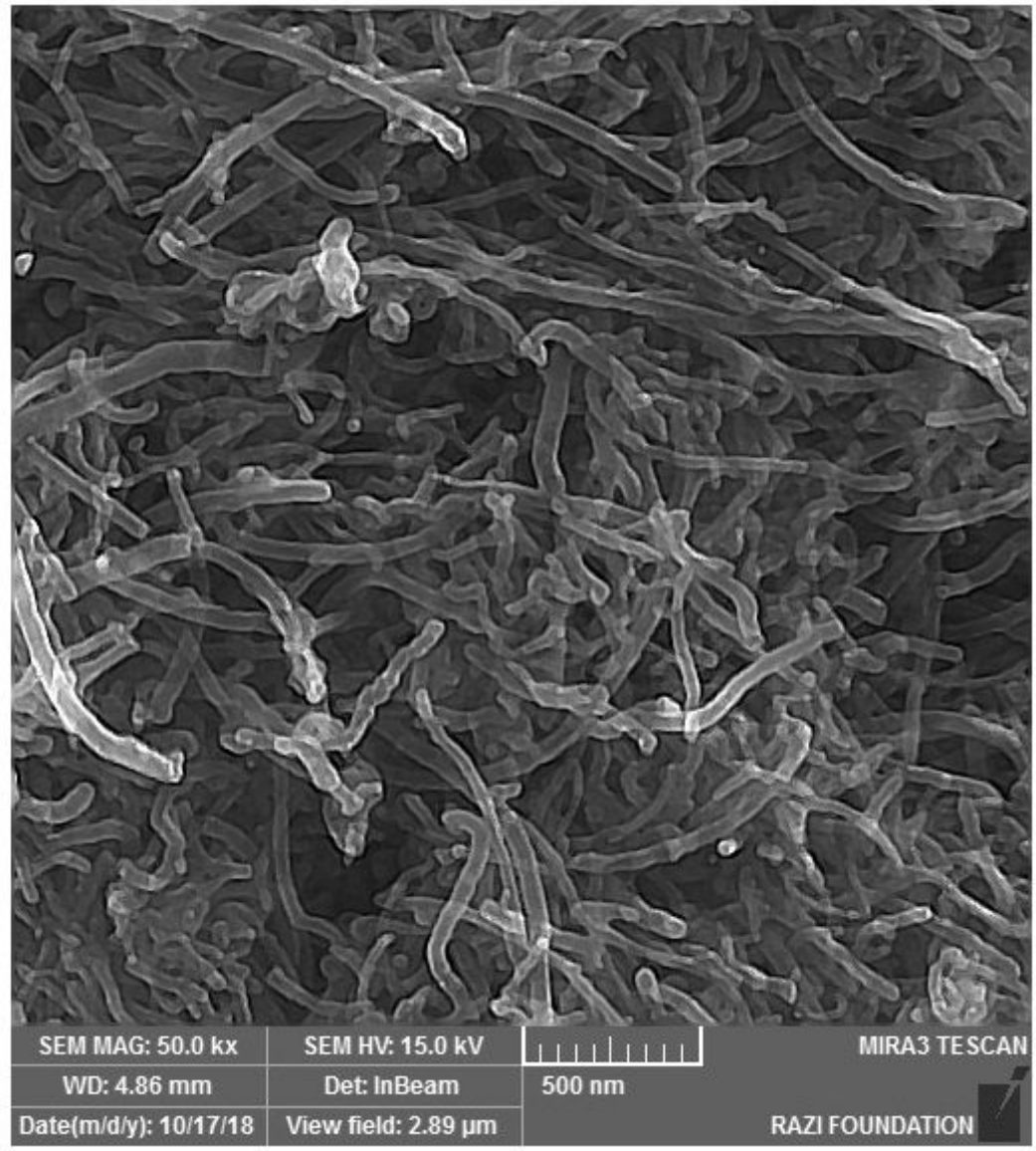

Figure 1

SEM image of the CNTs

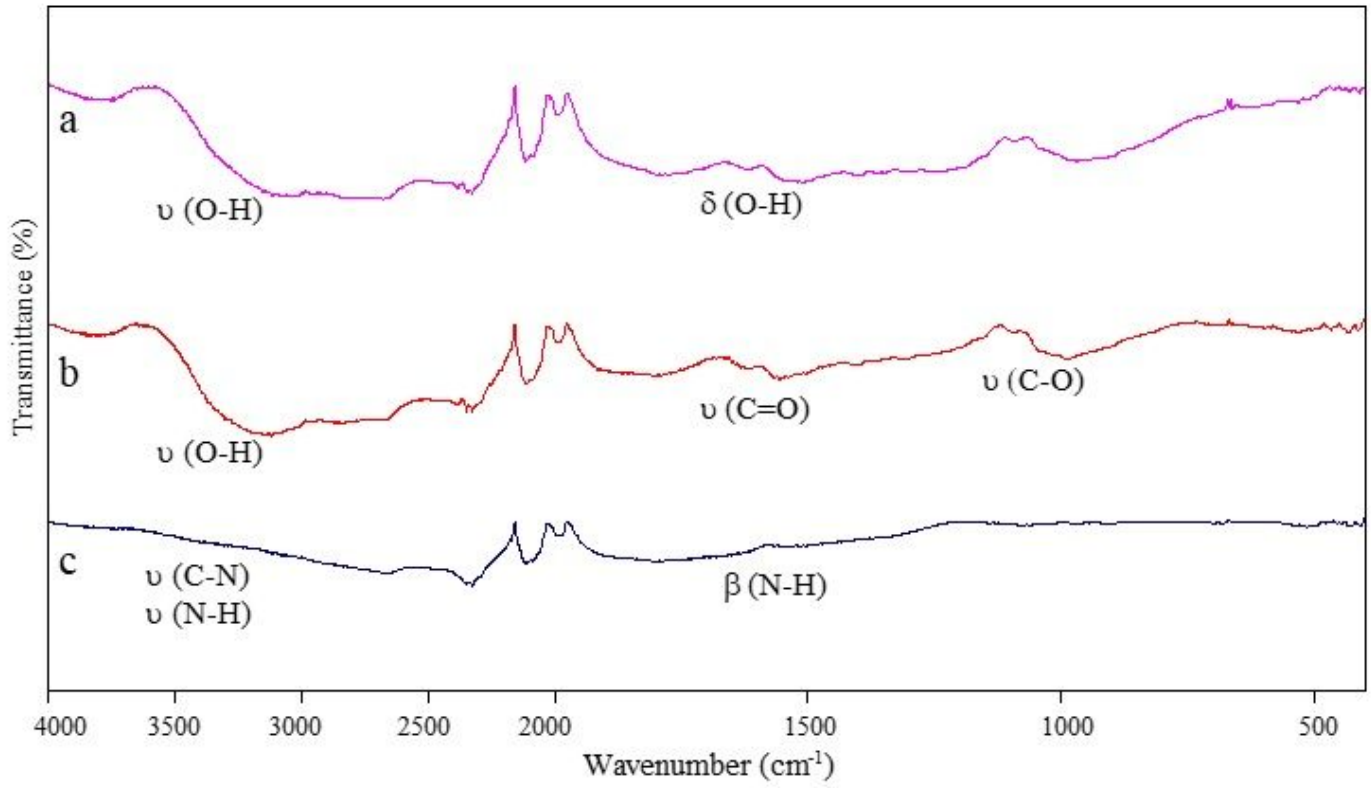

Figure 2

FTIR spectra of the CNT powders containing functional groups of a) OH, b) COOH, and c) NH2

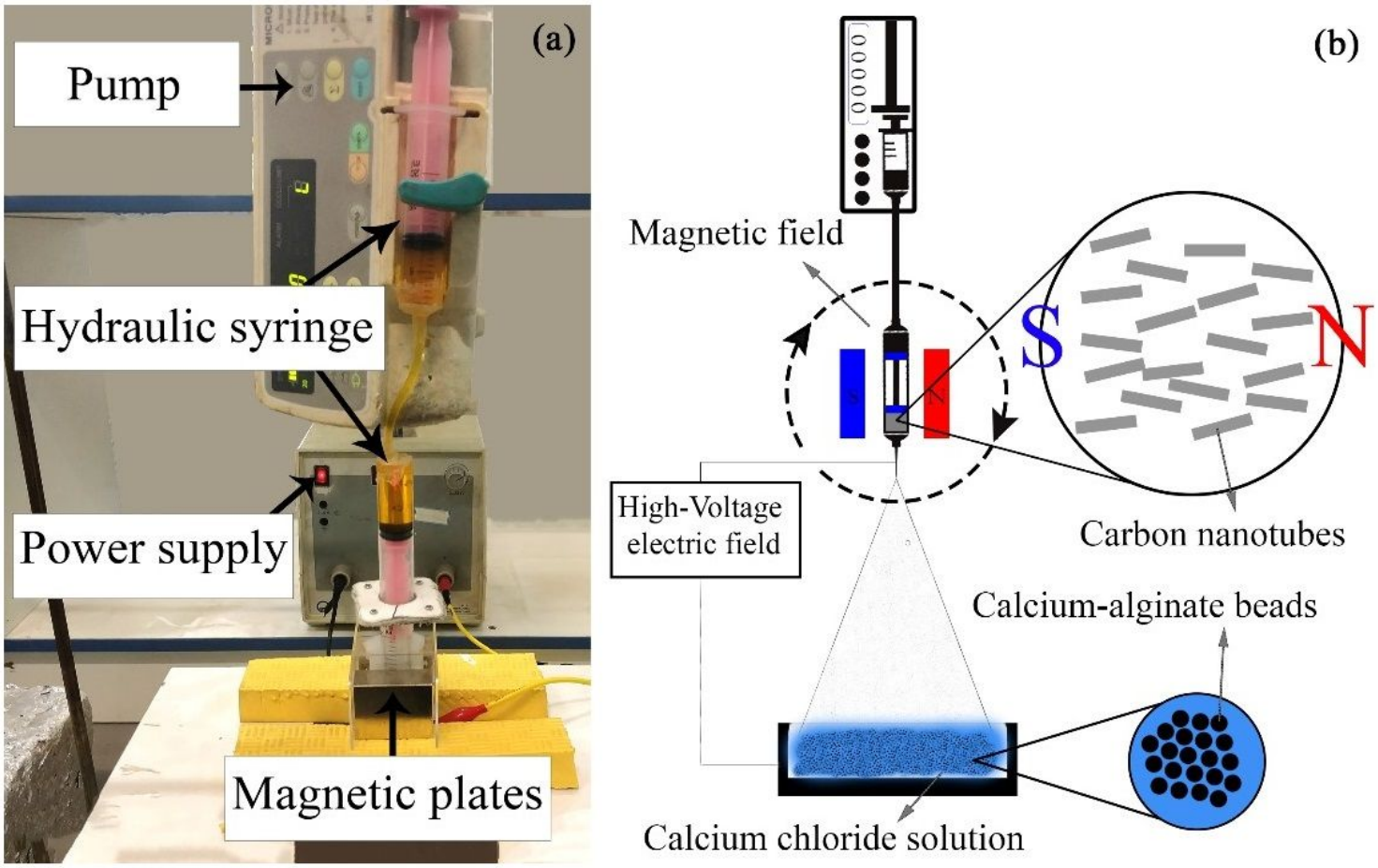

Figure 3

The experimental set up of the wet vertical electro-spraying system (a), and the schematic of the magnetic field

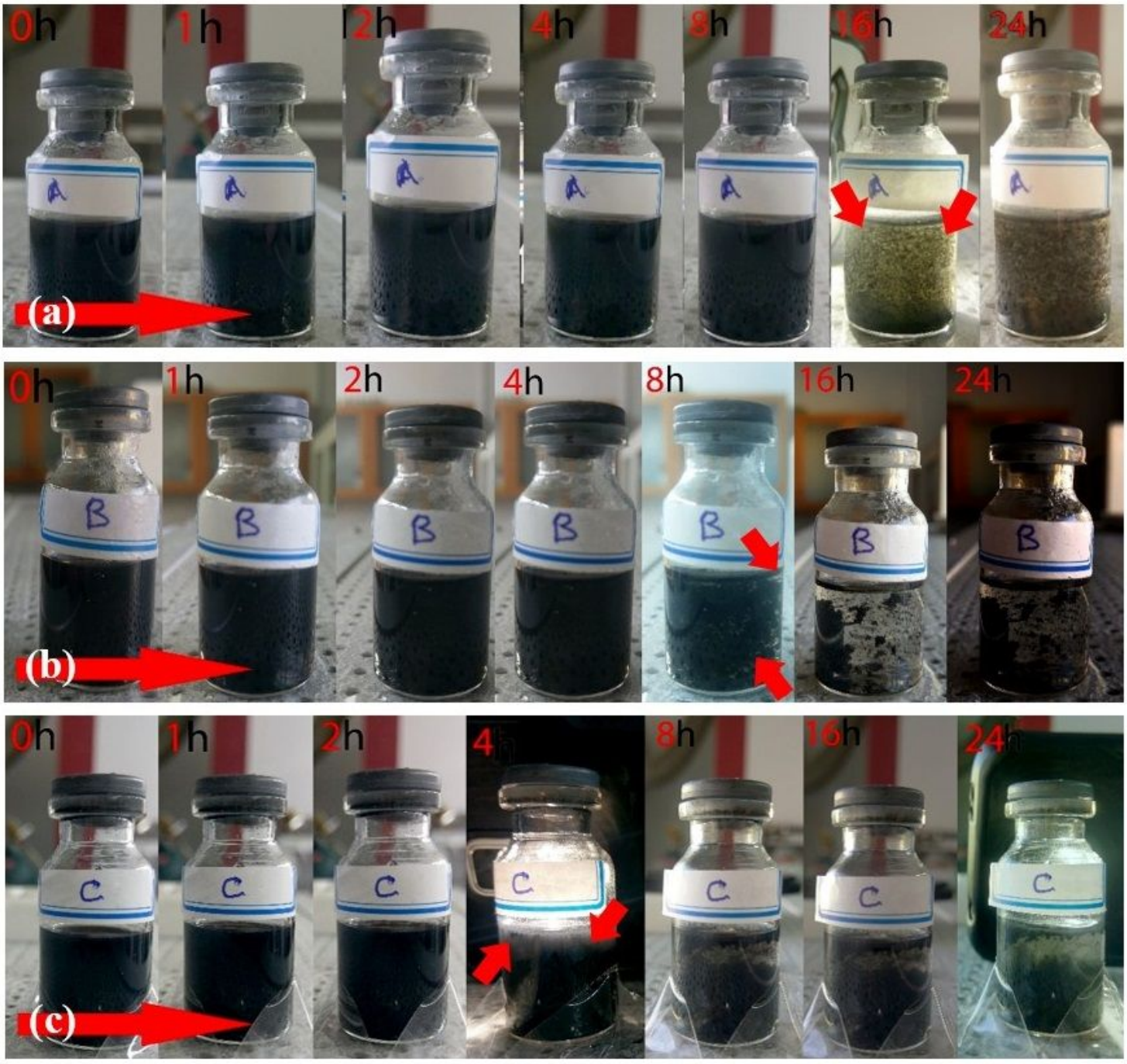

Figure 4

The results of the sedimentation rate test for the prepared SA-CNT samples a) CNT-OH, b) CNT-COOH, and c) CNT-NH2

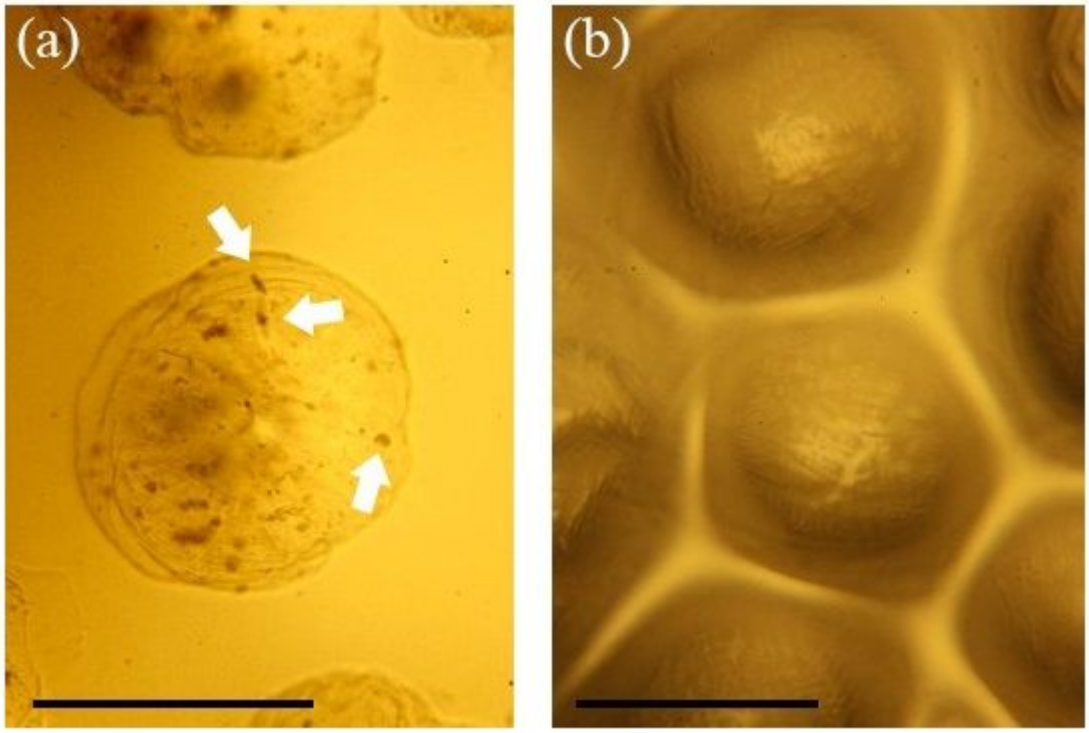

Figure 5

The optical images from the adsorbents prepared by the (a) unstable, and (b) stable solutions of the CNTs. The scale bar is 500 μm

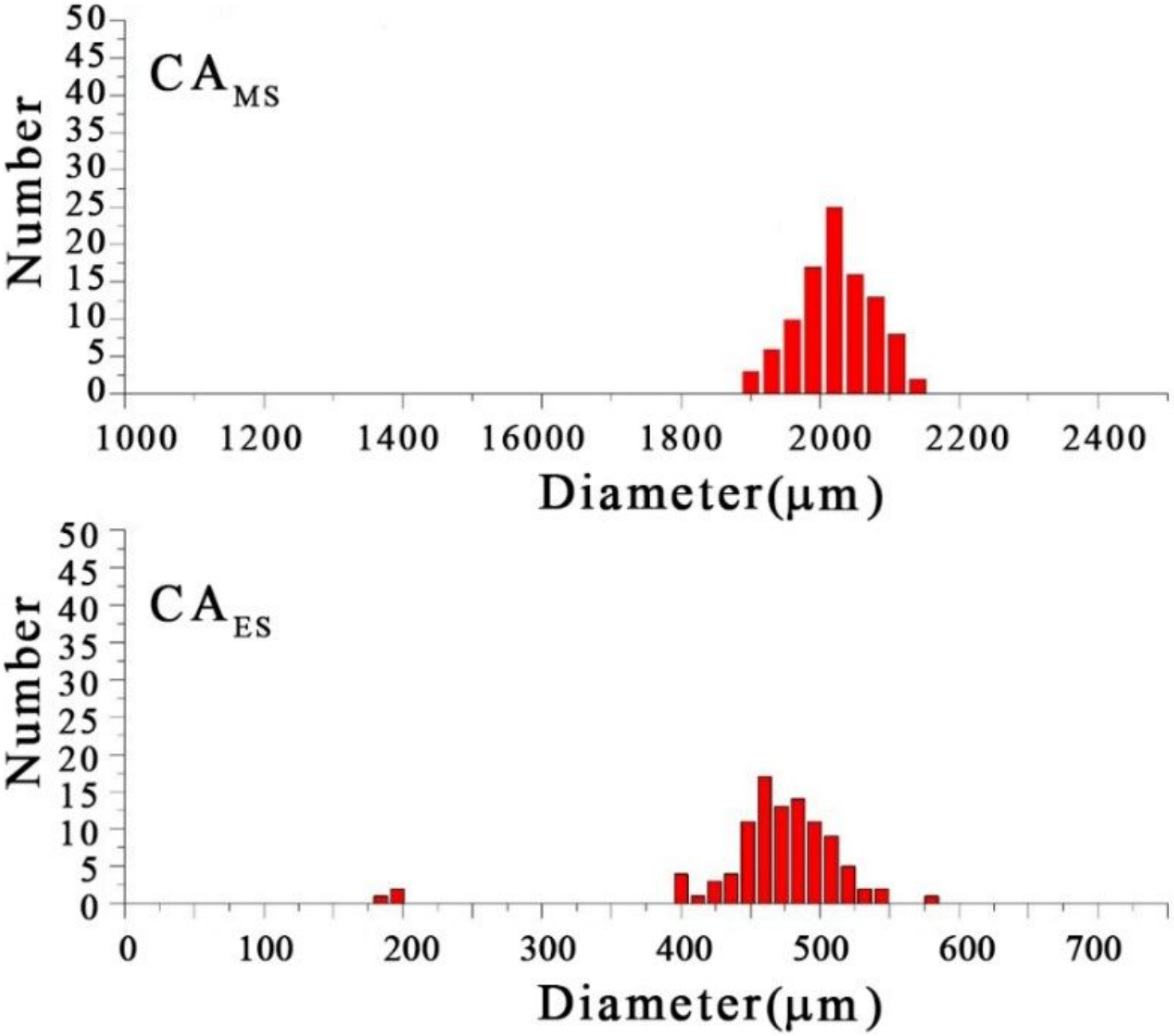

Figure 6

The bead-size distribution graphs of the CAMS and CAES adsorbents

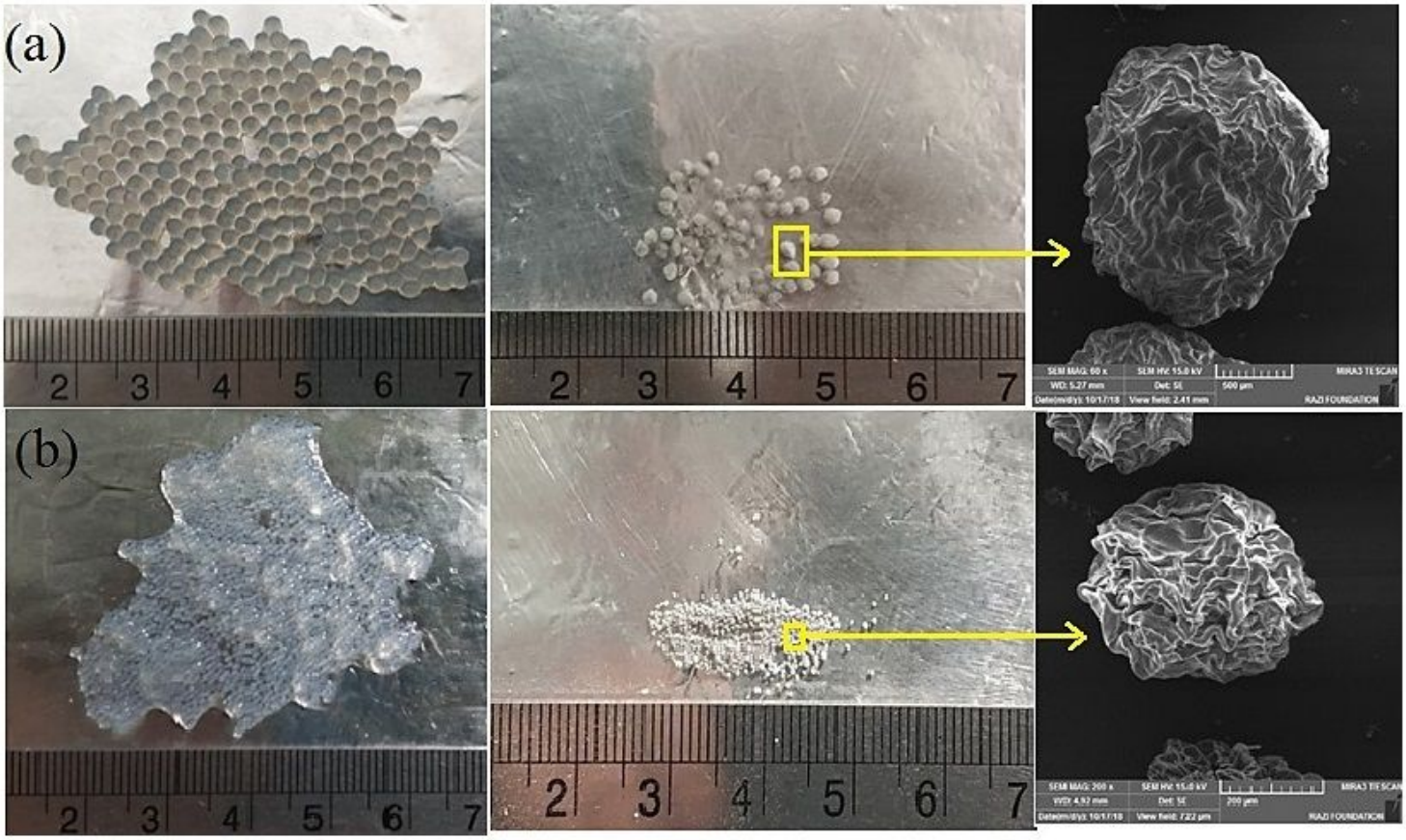

Figure 7

Bead images before and after the freeze drying a) mechanical spray b) electrospray

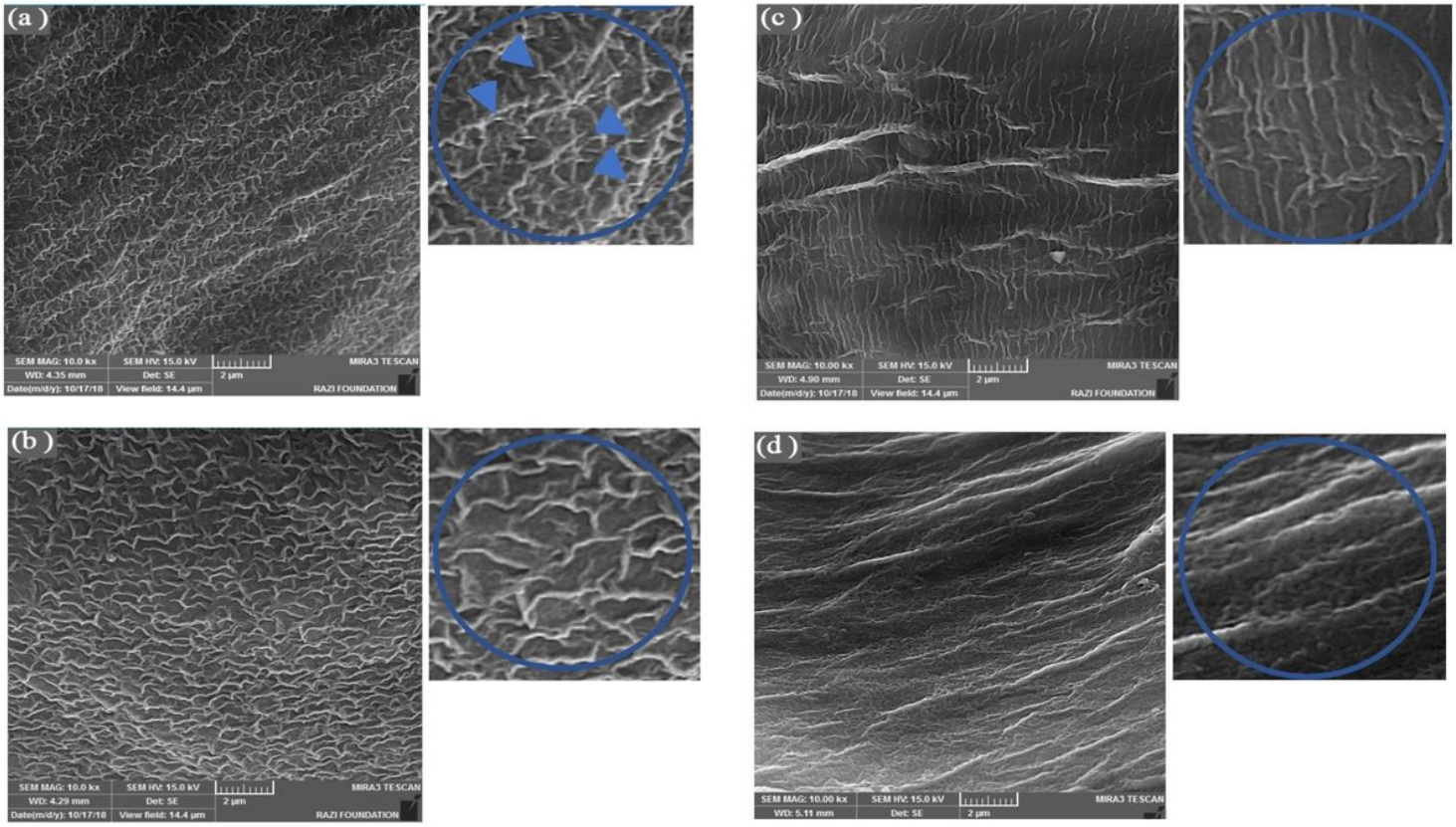

Figure 8

SEM images from the outer surfaces of the (a) CA-CNTMS, (b) CA-CNTM/MS, (c) CA-CNTES, and (d) CA-CNTM/ES samples

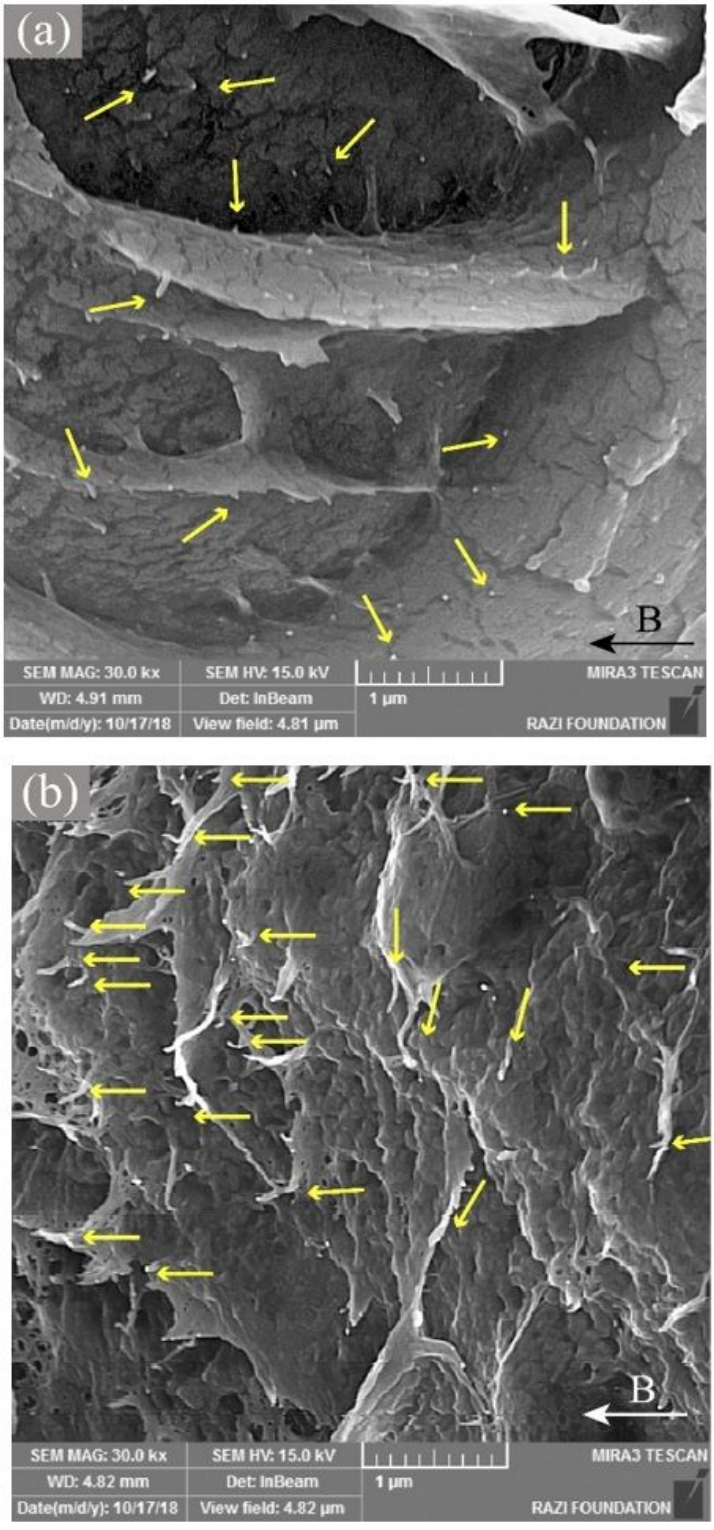

Figure 9

The fractured surfaces of the (a) CA-CNTES and (b) CA-CNTM/ES samples. The yellow arrows indicate the direction of the CNTs

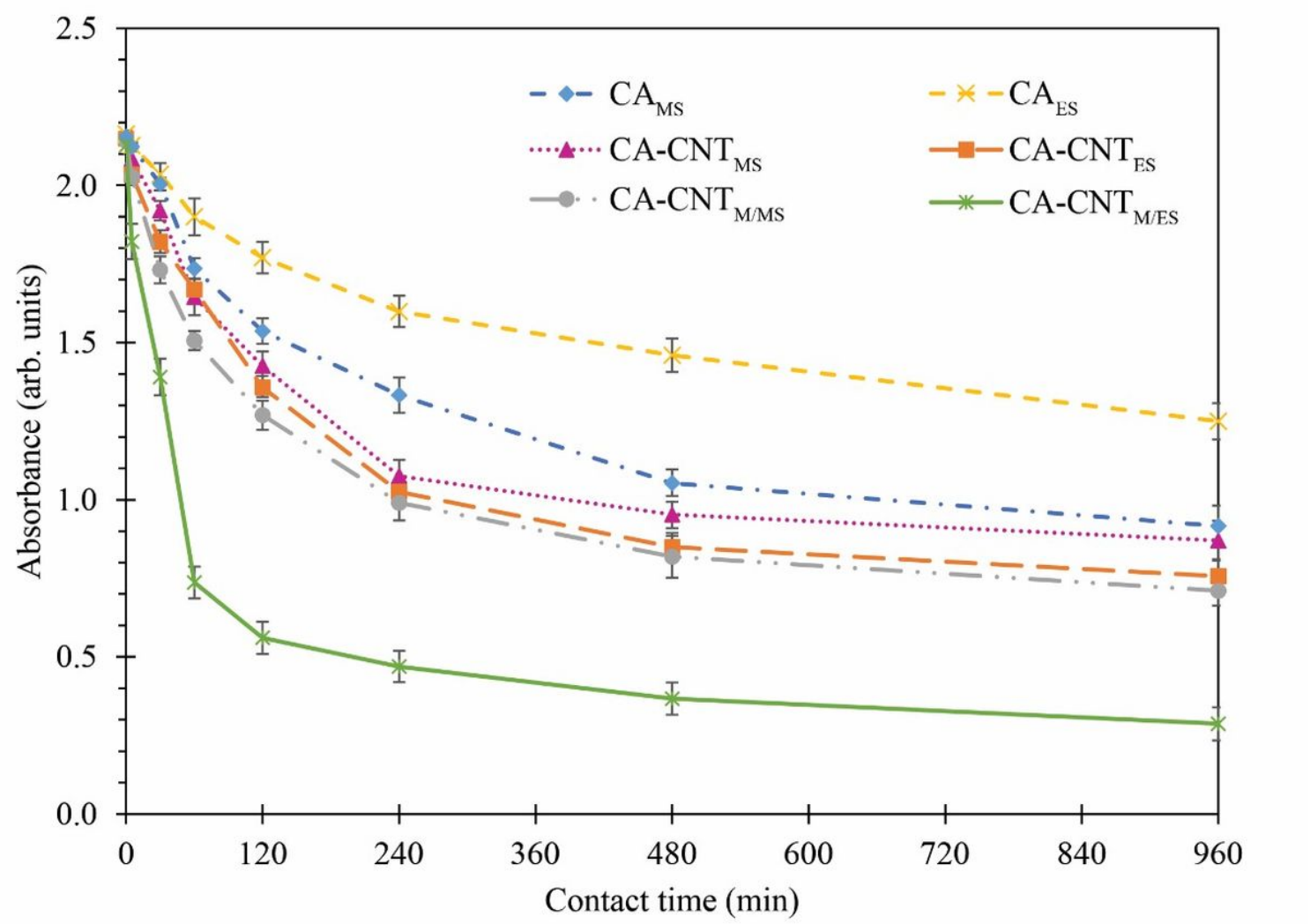

Figure 10

The adsorption spectrum of the MB solution as a function of the contact time for the six fabricated beads

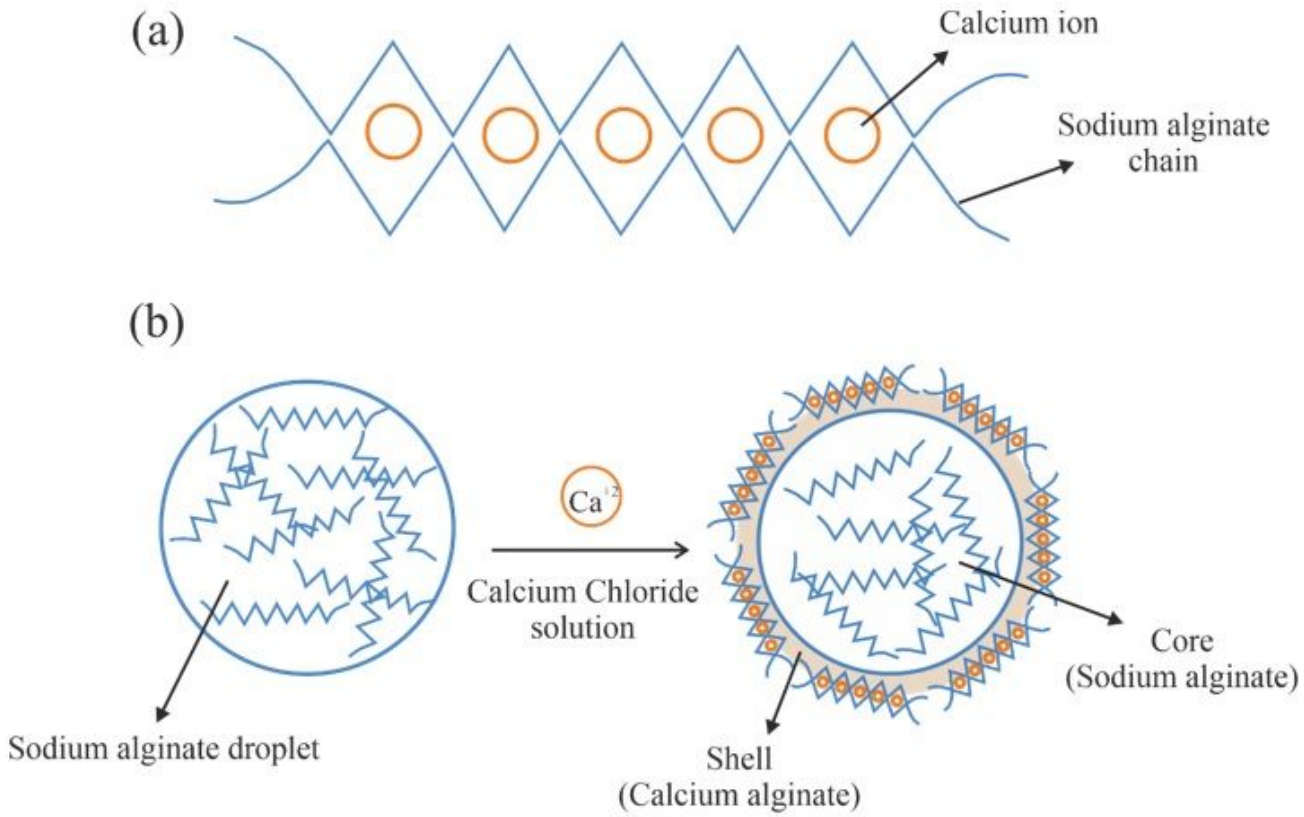

Figure 11

The egg-box model (a). Production of calcium alginate core-shell particle by dripping sodium alginate solution in calcium chloride solution (b)

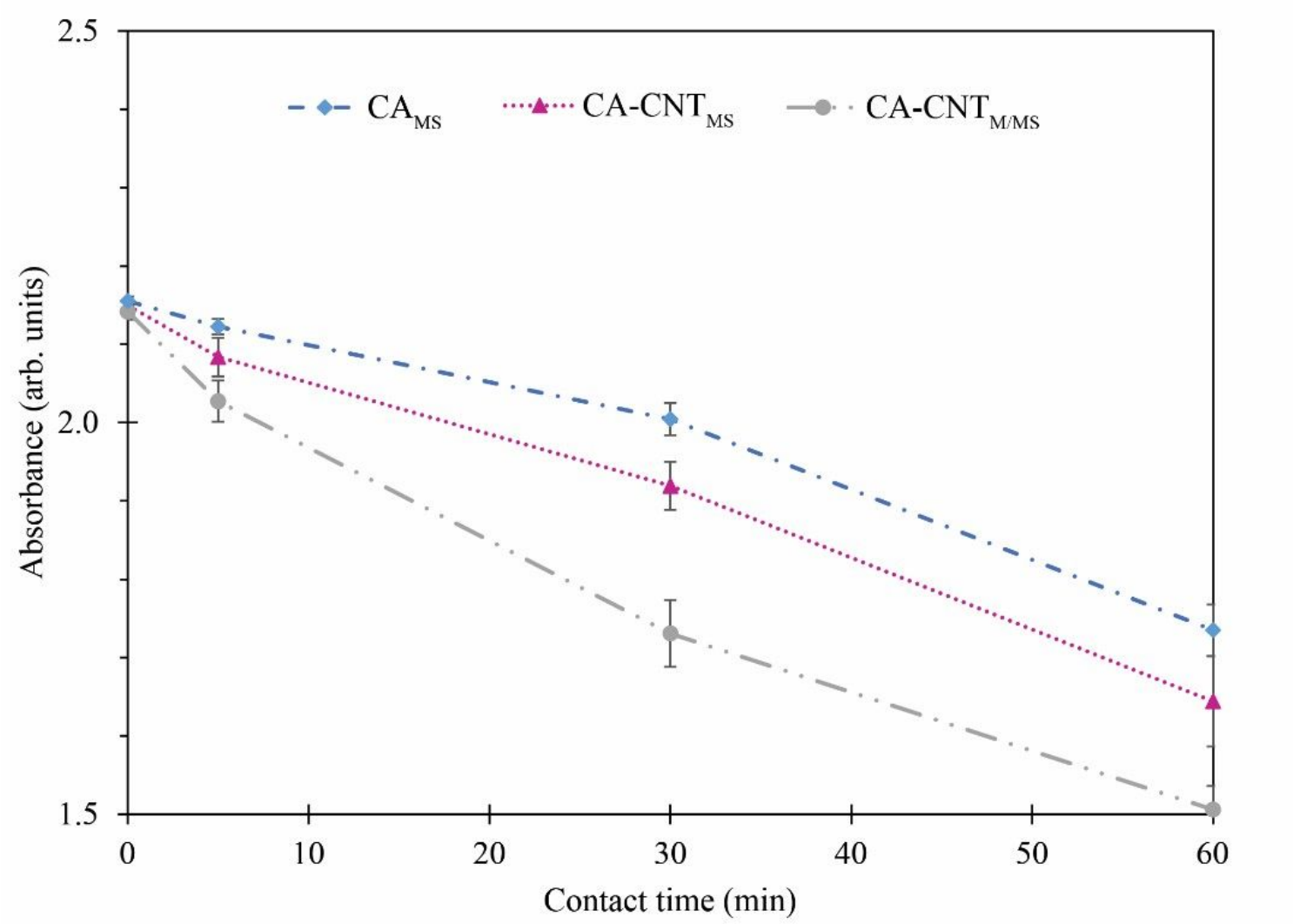

Figure 12

The adsorption spectrum of the MB solution as a function of the contact time for the samples produced by the mechanical spraying

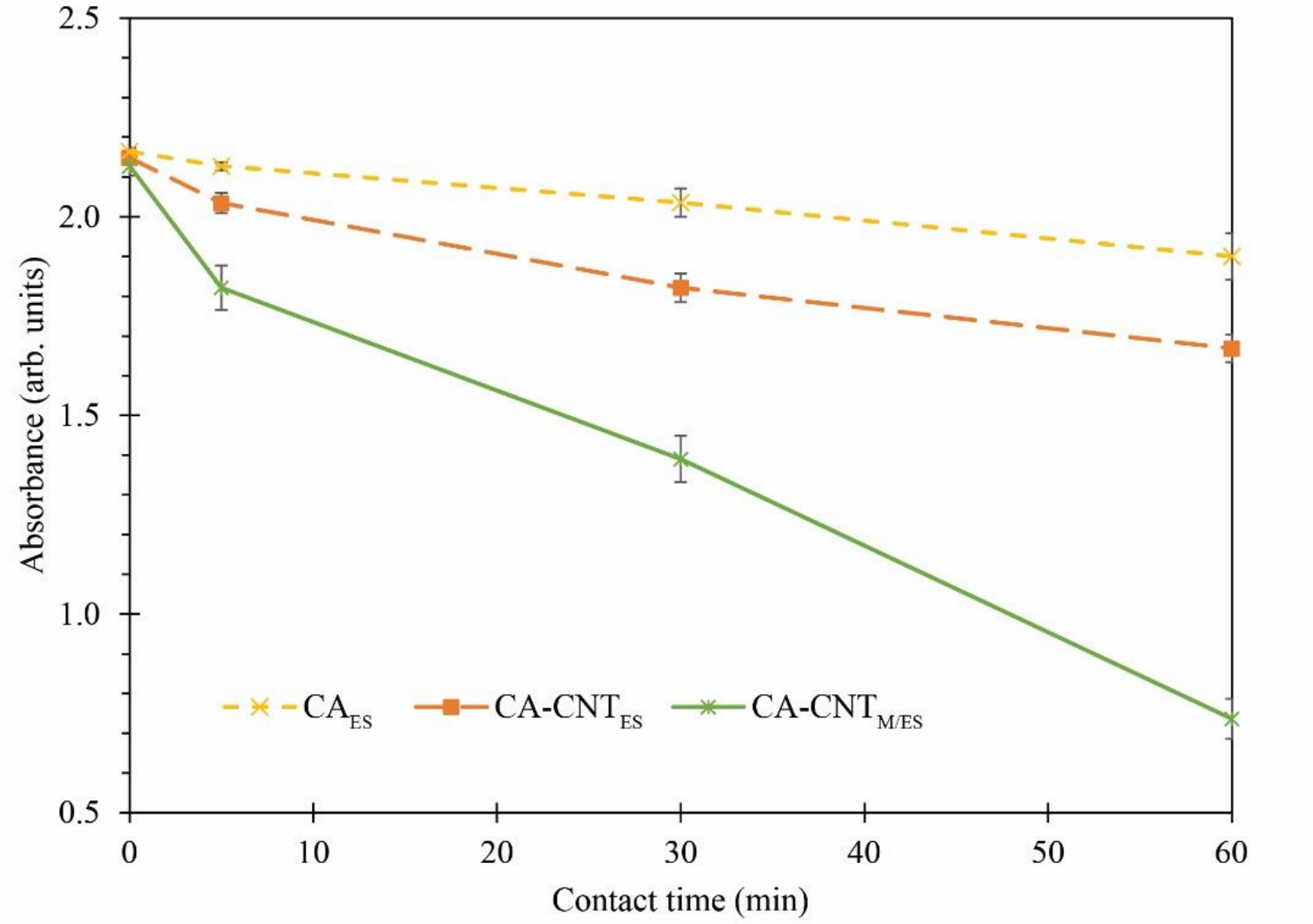

Figure 13

The adsorption spectrum of the MB solution as a function of the contact time for the samples produced by the electro-spraying